frontiers in Energy Research

ORIGINAL RESEARCH
published: 06 October 2021
doi: 10.3389/fenrg.2021.729919

Enhanced Reforming of Tar Based on Double-Effect Ni/CaO–$Ca_{12}Al_{14}O_{33}$ Catalysts: Modified by Ce, Mg, and Fe

Panlei Wang[1,2], Weidong Zhang[2], Zhenyu Yu[2], Huaqing Xie[2], Mi Zhou[1,2]* and Zhengyu Wang[2]*

[1]Key Laboratory of Metallurgical Emission Reduction and Resources Recycling, Ministry of Education (Anhui University of Technology), Maanshan, China, [2]School of Metallurgy, Northeastern University, Shenyang, China

The double-effect Ni-based catalysts, modified with Ce, Mg, and Fe and synthesized by the coprecipitation method, were applied into the enhanced steam reforming process of real tar. The effects of the catalysts with different doping mass proportions (3, 6, 9, and 12%) of Ce, Mg, and Fe on the H_2 yield, and H_2 and CO_2 concentrations were studied. The results revealed that the tar reforming efficiency was improved with appropriate proportions of the additives added. The Ce- or Mg-doped catalyst could change the distribution or morphology of the active component Ni. The modified catalyst with 6% Ce or 3% Mg doping showed the best catalytic activity in the reforming experiment, with the H_2 yield reaching 86.84% or 85.22%, respectively. The Fe-doped catalyst could form an Ni–Fe alloy and improve the stability of the catalyst, and the better catalytic activity can be obtained at 9 and 12% Fe doping, with the H_2 yield reaching 85.54 and 85.80%, respectively.

Keywords: tar, double-effect catalyst, CO_2 adsorption, enhanced reforming, hydrogen production

OPEN ACCESS

Edited by:
Akshat Tanksale, Monash University, Australia

Reviewed by:
Ningbo Gao, Xi'an Jiaotong University, China
Wenhao Wang, Guizhou University, China

****Correspondence:***
Huaqing Xie
huaqing_2008@163.com
Mi Zhou
zhoum@mail.neu.edu.cn

Specialty section:
This article was submitted to Advanced Clean Fuel Technologies, a section of the journal Frontiers in Energy Research

Received: *24 June 2021*
Accepted: *06 September 2021*
Published: *06 October 2021*

Citation:
Wang P, Zhang W, Yu Z, Xie H, Zhou M and Wang Z (2021) Enhanced Reforming of Tar Based on Double-Effect Ni/CaO–$Ca_{12}Al_{14}O_{33}$ Catalysts: Modified by Ce, Mg, and Fe. Front. Energy Res. 9:729919. doi: 10.3389/fenrg.2021.729919

INTRODUCTION

Coal gasification plays an important role in the coal chemical industry, while tar is the main by-product of this process. In China, the total output of coke was 473.1 million tons in 2019, with about 19 million tons of tar as the by-product. The composition of tar is complex, and it is estimated to include more than ten thousand compounds. Distinguish by boiling point, tar includes light oil, phenol oil, naphthalene oil, washing oil, onion oil, and coal tar pitch (Li and Suzuki, 2010; Li et al., 2013; Duan et al., 2017). Tar is gaseous at high temperature and liquid at low temperature, which will easily corrode the pipeline equipment. In addition, it can cause harm to the ecology and the human body if discharged into the environment (Xie et al., 2016a; Zeng et al., 2018; Li et al., 2021; Zuo et al., 2021). The methods of tar removal include physical and chemical methods. The physical method is to remove the tar from the syngas through the principle of absorption and adsorption, such as water washing, oil washing to absorb tar, or using porous media to adsorb tar onto its surface. The physical method has the advantages of simple operation and a low equipment cost, but there are some disadvantages such as secondary pollution and low removal efficiency (Xie et al., 2016c). The chemical method mainly includes the pyrolysis method and reforming method (partial oxidation reforming and steam reforming). The pyrolysis method refers to the tar cracking at high temperature to produce non-condensable small molecules of gas, which increases the cost due to the need of adding additional heat sources (Torres et al., 2007). The partial oxidation reforming method

can effectively convert tar into small molecular gases such as H_2 and CO, but the process is mainly conducted at a higher temperature (about 1,200°C), by consuming a large amount of pure oxygen and additional fuel to supply heat (Onozaki et al., 2006). The steam reforming method prefers to obtain hydrogen-rich gas under the action of steam and catalyst. Compared with the partial oxidation reforming method, the temperature of this method is lower (about 800°C), with no additional O_2 and less heat. Thus, steam reforming of tar and its model compounds for hydrogen production has received extensive attention in recent years (Furusawa et al., 2013; Duan et al., 2015; Li et al., 2015; Dou et al., 2016; Duan et al., 2018; Xie et al., 2018).

Catalysts are key to steam reforming of tar, and many catalysts have been studied so far. The commonly used catalysts mainly include dolomite (Gusta et al., 2009; Sarıoğlan, 2012), olivine (Virginie et al., 2012), alkali metal (Jiang et al., 2015), Ni-based catalysts (Richardson et al., 2010; Chan and Tanksale, 2014; Xie et al., 2015), and noble metal catalysts (Furusawa et al., 2013; Mei et al., 2013). Considering the catalyst efficiency and cost, the Ni-based catalyst is one of the most promising catalysts for tar reforming. However, inhibiting its carbon formation and improving its catalytic stability are the urgent problems to be solved (Yue et al., 2010; Gao et al., 2015). As a carrier, $Ca_{12}Al_{14}O_{33}$ can improve the reactivity and the anti-carbon property of the Ni-based catalyst. It itself can also be used as a catalyst for cracking tar, and the synergistic with Ni addition can further inhibit the carbon formation (Li et al., 2009). However, common steam reforming reactions yield only 70% (volume fraction) H_2 and more than 20% CO_2, limiting the use of such a hydrogen-containing gas (Xie et al., 2016d). So, researchers try to add adsorption components to the original catalyst and combine the catalytic reforming process with the CO_2 adsorption process. The adsorbent components can break the balance of the original reforming reaction, improving the quality and concentration of H_2, and the carbon deposition on the catalyst can be effectively reduced (Kinoshita and Turn, 2003; Dou et al., 2016; Xie, et al., 2016b; Zuo et al., 2020). In the adsorption-enhanced process, CaO is widely used as the CO_2 adsorbent due to its low cost and easy accessibility. However, CaO is easy to be sintered at high temperatures, resulting in a decrease in the adsorption capacity (Zamboni et al., 2011). As mentioned above, as a carrier, $Ca_{12}Al_{14}O_{33}$ has a special free oxygen storage structure, which can also effectively inhibit the sintering of CaO when carried within $Ca_{12}Al_{14}O_{33}$ (Li et al., 2009). Thus, the double-effect Ni/CaO–$Ca_{12}Al_{14}O_{33}$ catalyst was prepared and applied to the steam reforming process of 1-methylnaphthalene ($C_{11}H_{10}$) as a tar model component in our previous study, showing a good catalytic activity and CO_2 adsorption capacity (Zhang et al., 2021a; Zhang et al., 2021b). However, the double-effect catalyst has not been applied in the reforming of real tar, and because of its component's complexity, the catalytic performance on the reforming process of real reforming may be decreased compared to that on the model component. According to the literature, the catalytic activity and anti-carbon property of the Ni-based catalyst can be improved by adding additives such as precious metals (Pt, Rh, Ru, etc.) (Mei et al., 2013; Cai et al., 2014), rare earth metals (La, Ce, etc.) (Kimura et al., 2006; Tomishige et al., 2007; Mazumder and Lasa., 2015), alkali earth metals (Ca, Mg, etc.) (Wang et al., 2006; Ashok et al., 2015; Nakhaei and Mousavi, 2015), and transition metals (Fe, Co, etc.) (Wang et al., 2011; Koike et al., 2012; Wang et al., 2013). Considering the cost, Ce (rare earth metal), Mg (alkali earth metal), and Fe (transition metal) were studied in this article.

In this article, modified double-effect Ni-based catalysts were prepared and applied to the enhanced reforming process of real tar. The double-effect Ni-based catalysts with different additives (Ce, Mg, and Fe) of different doping mass proportions (3, 6, 9, and 12%) were synthesized by the coprecipitation method and were characterized by X-ray diffraction (XRD) and scanning electron microscopy (SEM). Then, the effects of different modified double-effect catalysts on the hydrogen production from the enhanced reforming of tar were studied, and the result was compared with that over the unmodified double-effect Ni-based catalyst.

EXPERIMENTAL

Tar Sample

The raw tar sample came from a coking plant in Liaoning province, China. The sample was preheated by distillation to remove moisture and solid-phase impurities prior to the chemical composition analysis. Elementar (vario MACRO cube, Germany) was used for the elemental analysis of tar, and the results show that the molar content of C is 54.50%, H is 39.27%, O is 5.32%, N is 0.70%, and S is 0.21%. The chemical formula of the sample can be simplified to $C_{10}H_{7.21}O_{0.98}$, ignoring nitrogen and sulfur that were too low compared with other elements. Therefore, the steam reforming (SR) reaction of tar can be expressed by the following equation:

$$\boldsymbol{C_{10}H_{7.21}O_{0.98} + 9.02H_2O \rightarrow 10CO + 12.625H_2\ \Delta H > 0} \quad (1)$$

and following the water–gas shift (WGS) reaction, we obtain

$$\boldsymbol{CO + H_2O \rightarrow CO_2 + H_2\ \Delta H < 0} \quad (2)$$

Thus, the total steam reforming reaction can be written as follows:

$$\boldsymbol{C_{10}H_{7.21}O_{0.98} + 19.02H_2O \rightarrow 10CO_2 + 22.625H_2\ \Delta H > 0} \quad (3)$$

GC-MS (Agilent 5975–7890A, Shanghai Tianmei) was used for the composition analysis of tar. Specific operating conditions are as follows: 1) Chromatographic conditions: Hp-5 chromatographic column; oven temperature program was as follows: maintain 1 min at 60°C as the starting temperature, heat to 280°C with the heating rate of 15 C/min, and maintain for 5 min; and He as the carrier gas with the shunt ratio of 1:100. 2) Mass spectrometry conditions: solvent delay for 4 min; ionization source: EI; electron bombardment energy: 70 eV;

TABLE 1 | Constituent analysis of tar.

Number	Component	Molecular formula	Mole content/%
1	Indane	C_9H_8	1.753
2	Indene	C_9H_{10}	1.241
3	Naphthalene	$C_{10}H_8$	47.213
4	2-Benzothiophene	C_8H_6S	1.045
5	Naphthalene, 1-methyl-	$C_{11}H_{10}$	5.433
6	Naphthalene, 2-methyl-	$C_{11}H_{10}$	2.154
7	Biphenyl	$C_{12}H_{10}$	1.280
8	Naphthalene, 2,7-dimethyl-	$C_{12}H_{12}$	0.881
9	Naphthalene, 1,4-dimethyl-	$C_{12}H_{12}$	0.796
10	Naphthalene, 2,6-dimethyl-	$C_{12}H_{12}$	0.488
11	Acenaphthene	$C_{12}H_{10}$	7.059
12	Dibenzofuran	$C_{12}H_8O$	4.255
13	Fluorene	$C_{13}H_{10}$	5.991
14	[1,1′-Biphenyl]-4-carboxaldehyde	$C_{13}H_{10}O$	0.612
15	Dibenzofuran, 4-methyl-	$C_{13}H_{10}O$	0.671
16	Dibenzothiophene	$C_{12}H_8S$	1.247
17	Phenanthrene	$C_{14}H_{10}$	10.978
18	Anthracene	$C_{14}H_{10}$	1.655
19	Phenanthrene, 1-methyl-	$C_{15}H_{12}$	0.435
20	4H-Cyclopenta[def]phenanthrene	$C_{15}H_{10}$	0.594
21	Fluoranthene	$C_{16}H_{10}$	2.698
22	Pyrene	$C_{16}H_{10}$	1.521

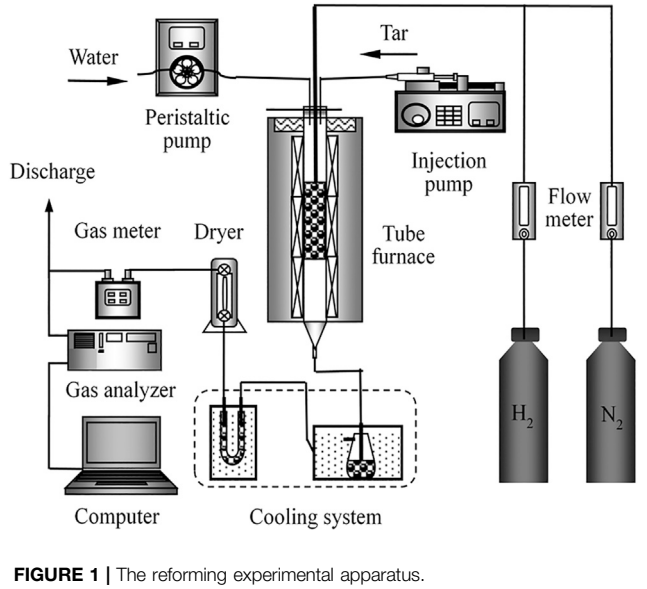

FIGURE 1 | The reforming experimental apparatus.

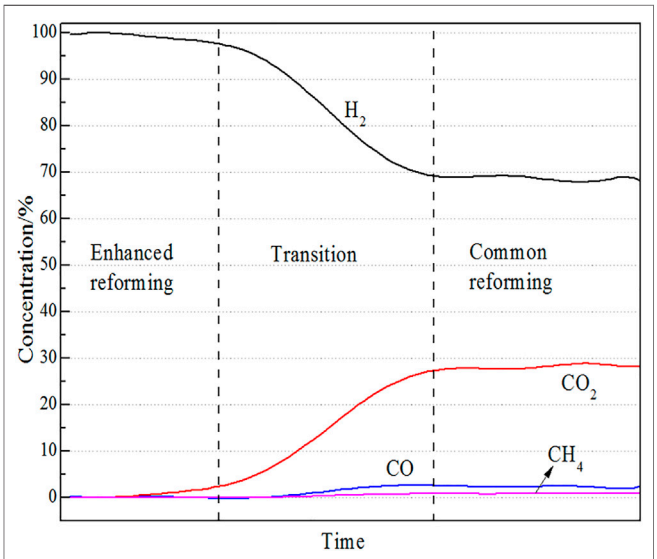

FIGURE 2 | Diagram of the reformed gas concentrations as a function of reaction time.

electronic multiplier voltage: 1200 V; and quality range: 30–600 amu, with the scanning interval of 0.5 s. Through the GC-MS analysis, a total of 22 major compounds were detected, among which the naphthalene content was the highest (given in **Table 1**).

Catalyst Preparation

The modified double-effect Ni-based catalysts were prepared by the coprecipitation method, with the mass proportion of Ni (catalytic component):CaO (adsorption component): $Ca_{12}Al_{14}O_{33}$ (carrier component) being 15:70:15. Meanwhile, Ce (Mg or Fe) was doped as the additive, with mass proportions of 3, 6, 9, or 12%. The catalyst preparation process needed to undergo a series of dissolving, stirring, drying, and calcination processes as follows: First, $Ca(CH_3COO)_2$ was calcined at 900°C for 2 h, to obtain high-activity CaO. Second, a certain quality of CaO, $Al(NO_3)_3\,9H_2O$, $Ni(NO_3)_2\,6H_2O$, and Ce (or Mg, Fe) were mixed with deionized water to form a suspension. Then, the suspension was stirred for 3 h, dried for 12 h at 120°C, and then calcined at 500°C for 3 h. Afterward, the calcined solid was cooled and formed into a suspension by adding deionized water again, followed by stirring and drying. Finally, the dried solid was calcined at 1,000°C for 4 h to obtain a catalyst.

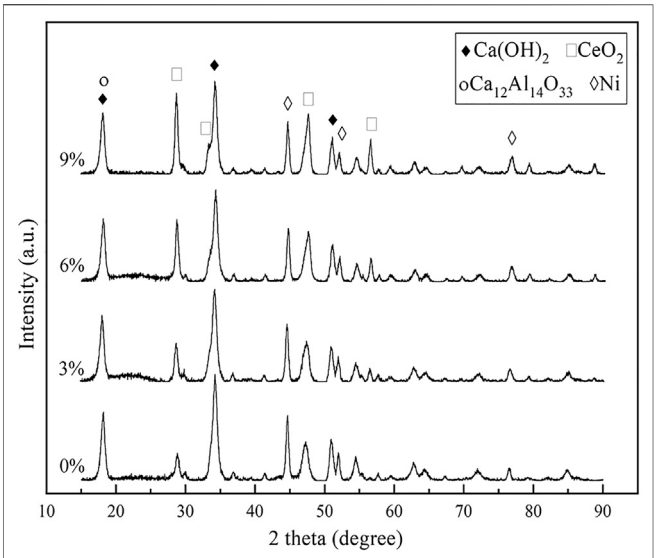

FIGURE 3 | XRD patterns of Ce-modified catalysts with different doping mass proportions.

Experimental Apparatus

The experimental apparatus for the reforming experiment is shown in **Figure 1**. The modified double-effect catalyst was kept in a three-stage temperature control tube furnace. The tar and deionized water were pumped into the stainless-steel downstream reactor drop by dropping through an injection pump and a peristatic pump with 600 ml/min N_2 carrier gas. To ensure the good fluidity of tar, the syringe was wrapped with a heating belt, keeping the wall temperature above 50°C. The product gas in the reactor was cooled and dried successively, and finally detected by a gas meter and a gas analyzer.

Experimental Design and Assessment

In this article, the catalytic performances of the modified double-effect catalysts were assessed under the optimal experimental condition based on the previously enhanced reforming experiment result with the unmodified catalyst (temperature = 740°C, S/C (the mole ratio of steam to carbon in tar) = 15, and WHSV (weight hourly space velocity) = 0.0447 h^{-1}).

The experimental process of the tar reforming can be divided into two stages: enhanced reforming stage and common reforming stage (shown in **Figure 2**). For the enhanced reforming stage, CO_2 generated via the WGS reaction (**Eq. 2**) was adsorbed by CaO in the double-effect catalyst (adsorption reaction, **Eq. 4**). Then, the equilibriums of the steam reforming reactions of tar were transferred to the direction of hydrogen production, with the CH_4 and CO concentrations being very low and the H_2 concentration being quite high. As the time went by, the concentration of CO_2 was increased and that of H_2 was decreased because the CO_2 adsorption capacity of the double-effect catalyst tended to be saturated. Finally, the H_2 and CO_2 concentrations tended to be stable, about 70 and 25%, respectively, which were similar with those of the dry reformed gas without adding any CO_2 adsorbent, and thus, such a stage was considered as a common reforming stage (Xie et al., 2018; Zhang et al., 2021b),

$$\boldsymbol{CO_2 + CaO \rightarrow CaCO_3\ \Delta H < 0} \quad (4)$$

The main indicators in this article were as follows.

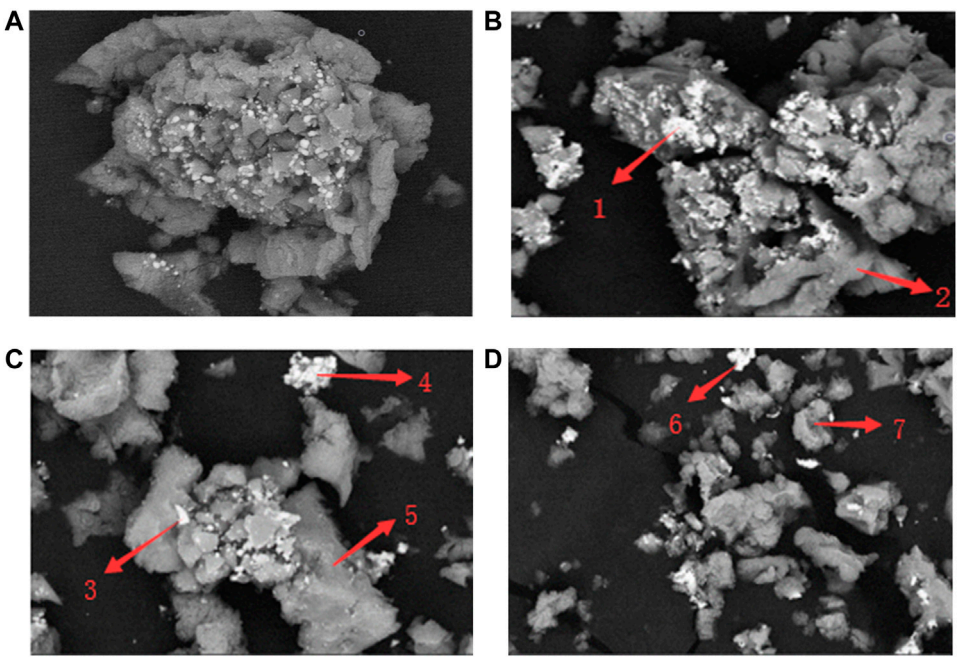

FIGURE 4 | SEM spectra of Ce-modified catalysts with different doping mass proportions: **(A)** 0%, **(B)** 3%, **(C)** 6%, and **(D)** 9%.

TABLE 2 | EDS table of Ce doped catalysts.

Element/%	O	Al	Ca	Ni	Ce
1	10.9	1.7	7.21	55.84	24.36
2	53.71	3.48	40.62	0.99	1.2
3	23.23	4.06	13.82	47.87	11.03
4	11	3.16	5.19	76.24	4.38
5	50.78	2.47	42.42	3.47	0.86
6	11.03	0.71	4.67	75.08	8.5
7	50.17	0.31	48.71	0.81	0

H_2 yield (Y_{H2}) was defined as the ratio of the output of H_2 ($Q_{H2,\ out}$) in the reformed gas to the theoretical output of H_2 (Q_{H2}) when all the input tar is converted completely via **Eq. 3**.

$$Y_{H_2} = \frac{Q_{H_2,out}}{Q_{H_2}} \times 100\% \tag{5}$$

The dry reformed gas ($Q_{total,\ out}$) was considered to be composed of H_2, CO, CO_2, and CH_4. The concentration of the reformed gas (C_i, i was H_2, CO, CO_2, or CH_4) was defined as the ratio of the output of i ($Q_{i,\ out}$) to the total output of the reformed gas ($Q_{total,\ out}$). In this article, only the concentrations of H_2 and CO_2 were studied in consideration of the extremely low concentrations of CO and CH_4,

$$C_i = \frac{Q_{i,out}}{Q_{total,out}} \times 100\% \tag{6}$$

RESULTS AND DISCUSSION

Effect of the Ce-Modified Double-Effect Ni-Based Catalyst

Catalyst Characterization Results

Prior to characterization, the prepared catalysts were activated at 800°C with 10% mol H_2/N_2 stream for 3 h. The structure of the catalysts was characterized by XRD (Shimazu, Japan, XRD-7000) using Cu Kα radiation operated at 30 kV and 40 mA, with the scanning angle of 10–80 rad and the scanning speed of 2 rad/min. The morphology of the catalysts was observed by SEM with the aid of a Hitachi su-8010 microscope.

Figure 3 shows the XRD patterns of Ce-modified catalysts with different doping mass proportions. As shown in the figure, the Ce-modified catalysts include the active components, Ni and CeO_2; adsorption component, $Ca(OH)_2$ (formed by CaO absorbing water in the air); and carrier component, $Ca_{12}Al_{14}O_{33}$. As the doping proportion increases, the peak value of CeO_2 significantly increased. **Figure 4** shows the SEM spectra of Ce-modified catalysts as well as the undoped sample

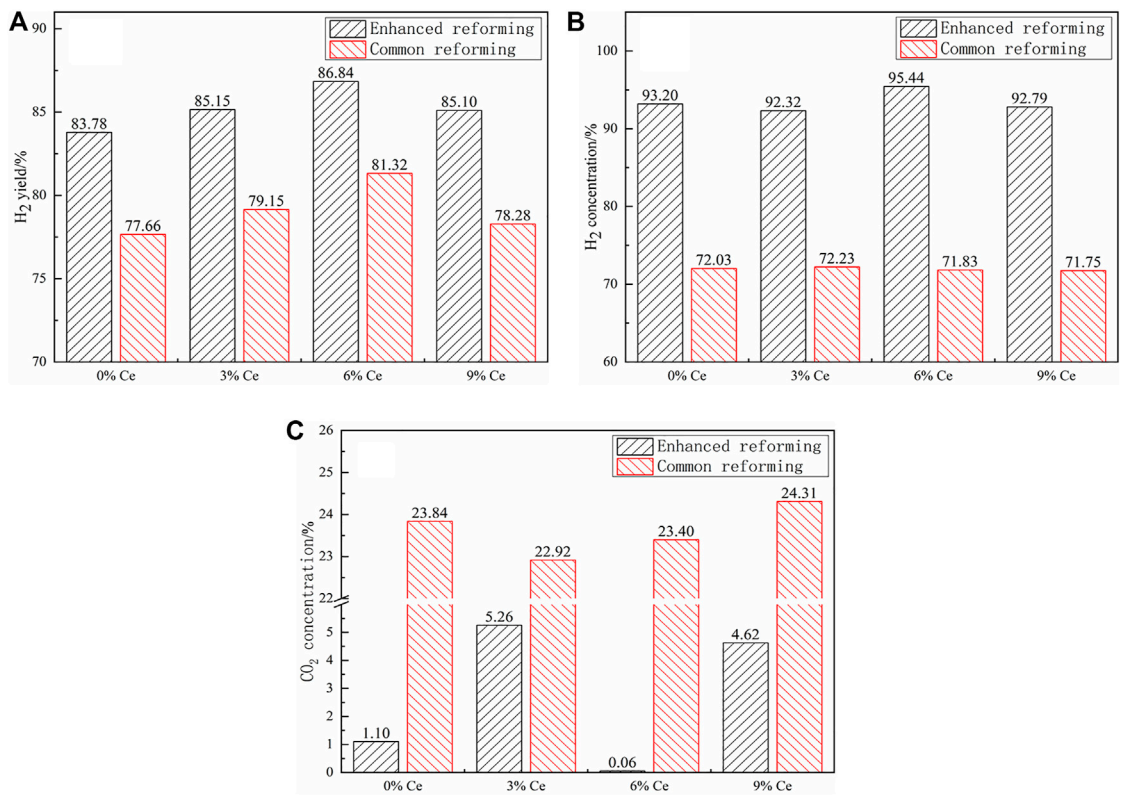

FIGURE 5 | Effect of the Ce-modified catalysts: **(A)** H_2 yield, **(B)** H_2 concentration, and **(C)** CO_2 concentration.

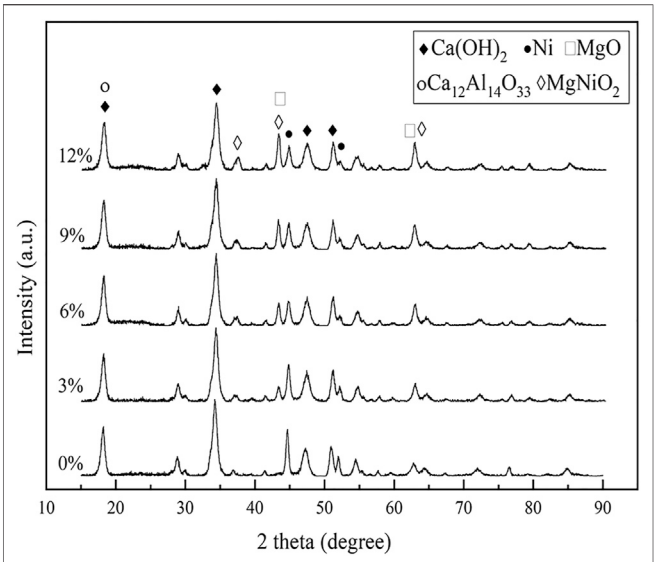

FIGURE 6 | XRD patterns of Mg-modified catalysts with different doping mass proportions.

(shown in **Figure 4A**). In the spectra, the bright part is mainly the active component Ni (shown by arrows 1, 3, 4, and 6), and the gray part is the adsorption component CaO and the carrier component $Ca_{12}Al_{14}O_{33}$ (shown by arrows 2, 5, and 7); the element contents of the different parts are shown in **Table 2**. The different particles were based on a CaO–$Ca_{12}Al_{14}O_{33}$ matrix, with Ni and CeO_2 dotting on the surface of the matrix by small spherical particles. Proper addition of Ce can improve the distribution of Ni, which showed that part of Ni no longer relied on or just relied on a small amount of the CaO–$Ca_{12}Al_{14}O_{33}$ matrix after Ce doping, with the small particles of Ni–CeO_2 also slightly increased.

Reformation Result

CeO_2 generally has a strong oxygen storage capacity due to its face-centered cubic structure. CeO_2 can provide oxygen atoms to the adjacent nickel metal and promote the oxidation reaction of carbon intermediate products on nickel metal, thus improving the catalyst reactivity and reducing the formation of carbon deposition (Kimura et al., 2006; Tomishige et al., 2007).

Figure 5A shows the H_2 yields of tar reforming over the catalysts with different Ce doping mass proportions. Overall, the catalysts, H_2 yields, and concentrations at the enhanced reforming stage were higher than those at the common reforming stage. It could also be seen that Ce doped in the catalyst could improve the H_2 yield at both the stages. As the doping proportion rose, the H_2 yields in the two stages first increased, then decreased, and finally reached the highest at the doping proportion of 6% (86.84% for the enhanced reforming). It was corroborated that a small amount of Ce doping made the active component no longer completely rely on the CaO–$Ca_{12}Al_{14}O_{33}$ matrix, and the active component distribution was more uniform,

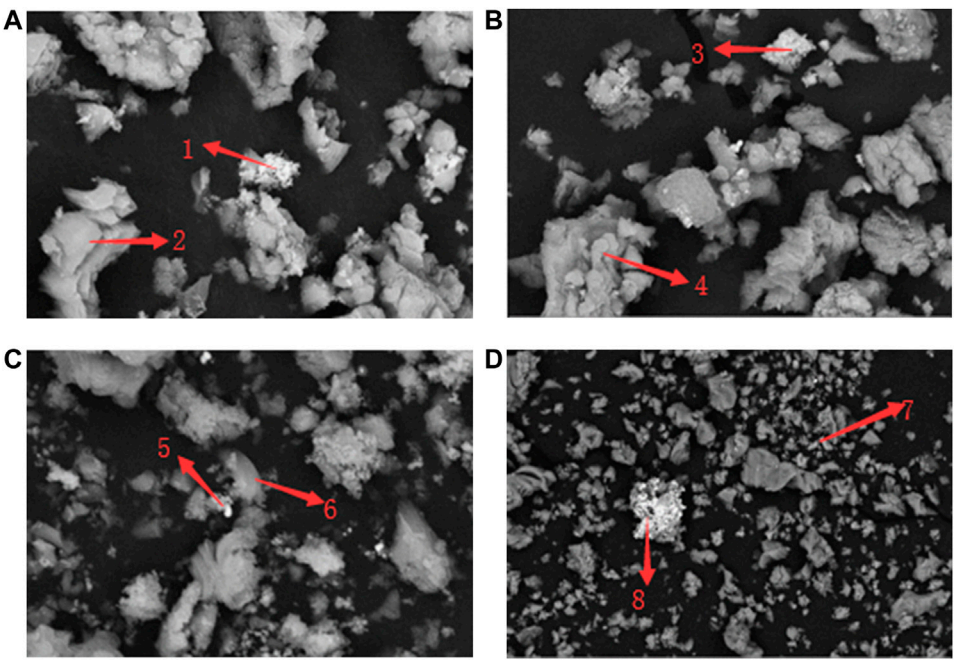

FIGURE 7 | SEM spectra of Mg-modified catalysts with different doping mass proportions: **(A)** 3%, **(B)** 6%, **(C)** 9%, and **(D)** 12%.

TABLE 3 | EDS of Mg doped catalysts.

Element/%	O	Mg	Al	Ca	Ni
1	23.6	10.57	5.13	9.5	51.2
2	41.5	0.28	0.58	56.89	0.75
3	19.27	17.46	2.25	4.88	56.15
4	68.58	1.23	1.98	19.08	9.12
5	12.03	3.64	3.22	7.43	73.68
6	41.74	10.22	10.54	17.71	19.78
7	21.75	20.23	2.54	12.08	43.4
8	29.44	24.61	3.17	6.54	36.24

thus promoting the SR reaction (**Eq. 1**), with the increase in the H_2 yield. However, the excessive Ce (>6%) doping produced more Ni and CeO_2 aggregated particles, which reduced the effective catalytic activity area, with the decrease in the H_2 yield. **Figures 5B,C** show the H_2 and CO_2 concentrations obtained over the catalysts with different Ce doping proportions. Due to the *in-situ* CO_2 adsorption, the H_2 concentrations of the enhanced reforming all over the catalysts with Ce doping were >90%, and among them, the sample with 6% Ce had the highest H_2 concentration (95.44%) and a very little CO_2 concentration, on some extent indicating that proper Ce addition can also improve the dispersion of CaO. After the adsorption saturation, i.e., at the common reforming stage, the H_2 concentrations were all about 72% and CO_2 concentrations were about 23–24%.

Effect of the Mg-Modified Double-Effect Ni-Based Catalyst

Catalyst Characterization Results

Figure 6 shows the XRD patterns of Mg-modified catalysts with different doping mass proportions. With the rise of the doping proportion, the peak value of Ni decreased, while those of MgO and $MgNiO_2$ spinels increased significantly. From **Figure 7** and **Table 3**, we can see that the CaO–$Ca_{12}Al_{14}O_{33}$ matrix was still the main composition in the catalyst (shown by arrows 2, 4, and 6), and the active components (shown by arrows 1, 3, 5, 7, and 8) on the matrix were changed from the original globular particles to spiny pellets, caused by the formation of $MgNiO_2$. With the rise of the doping proportions, the Mg-modified catalysts also showed the phenomenon that the active components detached from the CaO–$Ca_{12}Al_{14}O_{33}$ matrix and then aggregated alone, resulting in the decrease in the catalytic area (shown by arrows 7 and 8).

Reformation Result

Mg is a common additive in the process of steam reforming. MgO has a certain catalytic property and can also promote the oxidation of CO. For the Ni-based catalyst, the doping of Mg enables the catalyst to form one Ni–Mg–O solid solution, which has good stability and resistance to carbon deposition (Wang et al., 2006).

Figure 8 shows the H_2 yield and concentrations over the catalysts at different Mg doping proportions. For the two reforming stages, the

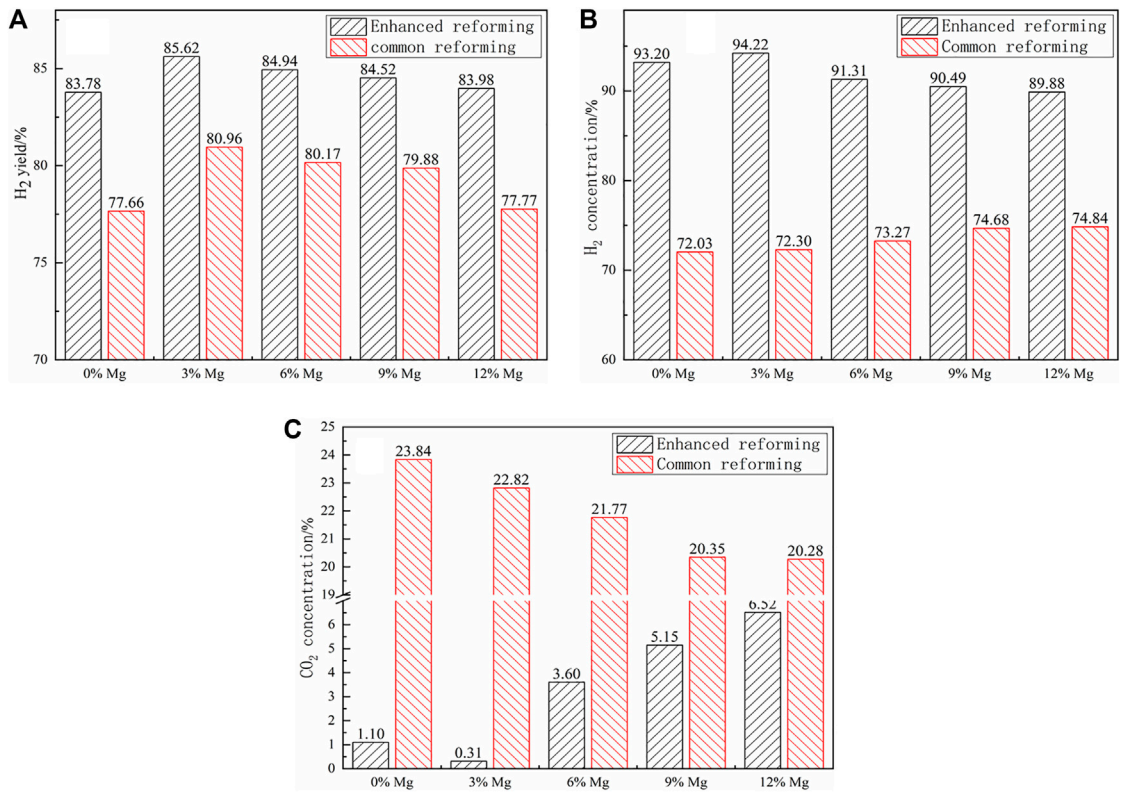

FIGURE 8 | Effect of the Mg-modified catalyst: **(A)** H_2 yield, **(B)** H_2 concentration, and **(C)** CO_2 concentration.

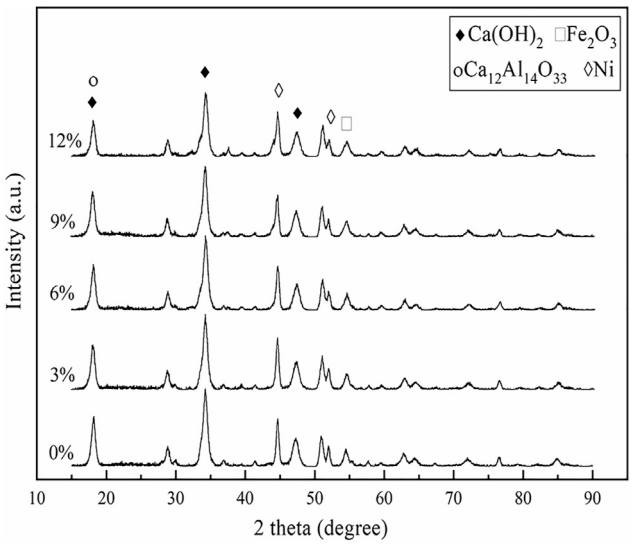

FIGURE 9 | XRD patterns of Fe-modified catalysts with different doping mass proportions.

addition of Mg can improve the SR reactions, with the increase in the H_2 yield. However, for the Mg-doped samples, the H_2 yield gradually decreased with the increase in the doping proportion. For the enhanced reforming, the H_2 yield reached the highest, 85.62%, at the doping proportion of 3%, and the H_2 concentration also decreased gradually with the rise of the Mg doping proportion in the enhanced reforming stage, and reached 93.20% at the doping proportion of 3%. Compared with the undoped catalyst, the increase in the H_2 yield and concentration corroborated that the increase in the catalytic area, causing the active components to change from the original globular particles to spiny pellets, promoted the SR reaction. Then, the decrease in the H_2 yield and concentration was because too much of the Mg-doped catalyst caused the active components to detach and aggregate, reducing the catalytic area. In the enhanced reforming stage, the CO_2 concentration gradually increased with the rise of the Mg doping proportion, to some extent corroborating the result found in the literature that doping Mg in the catalyst could promote the oxidation of CO (Wang et al., 2006). For the common reforming, Mg addition showed a slight increase in the H_2 concentration and a slight decrease in the CO_2 concentration with the increase in the doping proportion, which almost had no effect.

Effect of the Fe-Modified Double-Effect Ni-Based Catalyst

Catalyst Characterization Results

Figure 9 shows the XRD patterns of Fe-modified catalysts with different doping mass proportions. The XRD spectra of Fe-modified catalysts were similar to those of unmodified catalysts, and the peak value of Fe_2O_3 was weak and nearly did not change with the rise of the doping proportion. The SEM spectra and EDS results of Fe-modified catalysts are shown in **Figure 10** and **Table 4**. It could be seen that Ni (shown by arrows 1, 3, 5, 7, and 8) adhered to the surface of the CaO–$Ca_{12}Al_{14}O_{33}$ matrix (shown by arrows 2, 4, 6, and 8) in a

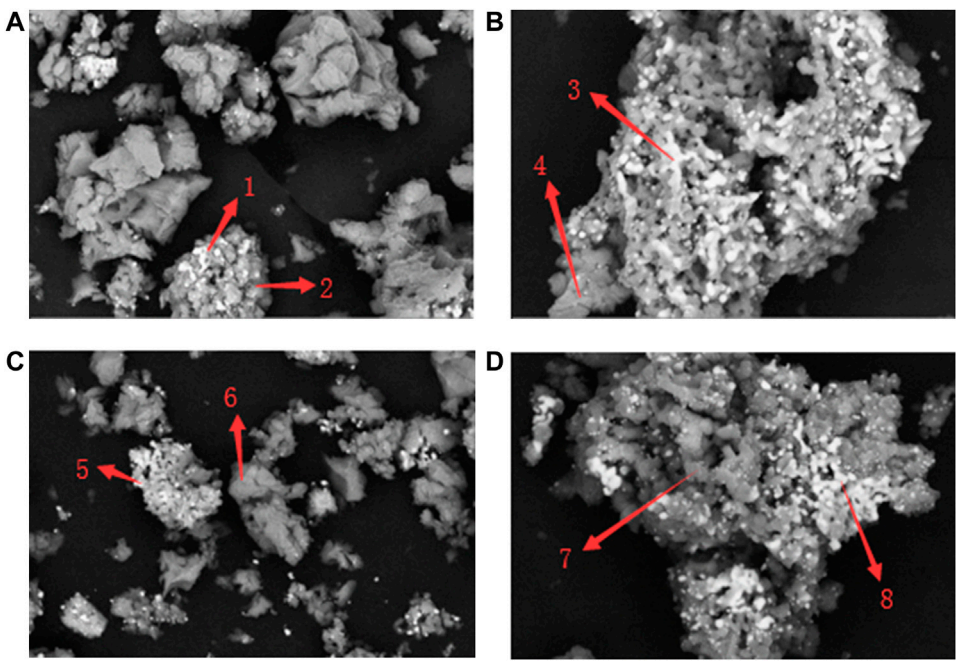

FIGURE 10 | SEM spectra of Fe-modified catalysts with different doping mass proportions: **(A)** 3%, **(B)** 6%, **(C)** 9%, and **(D)** 12%.

TABLE 4 | EDS of Fe doped catalysts.

Element/%	O	Al	Ca	Fe	Ni
1	14.01	2.5	14.36	1.7	67.43
2	41.49	2.46	52.32	0.38	3.35
3	5.48	2.59	3.55	5.29	83.09
4	45.43	1.83	39.6	1.64	11.5
5	6.89	1.57	4.71	1.5	85.33
6	33.67	8.94	30.59	19.37	7.43
7	15.3	1.14	5.41	50.42	27.74
8	31.08	6.41	28.12	4.49	29.9

granular form. Fe was uniformly distributed in the $CaO–Ca_{12}Al_{14}O_{33}$ matrix (shown by arrows 6 and 7), and different doping mass proportions of Fe had little effect on the distribution of the active component Ni.

Reformation Result

The oxide of Fe can be used as a catalyst for the reforming reaction, and its catalytic activity is lower than that of the Ni-based catalyst. For example, the active component of olivine is mainly Fe_2O_3. Ni and Fe can closely combine to form a Ni–Fe alloy and improve the stability of the catalyst. In addition, Fe doping in the catalyst can provide oxygen to neighboring nickel species and promote the oxidation of carbon, reducing the amount of carbon formation (Wang et al., 2011).

The effects of the modified catalysts on the H_2 yield and concentration are shown in **Figures 11A,B**. From the figure, it is clear that the H_2 yield and concentration gradually increased with the rise of the Fe doping proportion and then flattened out when the Fe doping proportion was over 9%. The H_2 yield of the enhanced reforming can reach 85.54 and 85.80% at the doping proportions of 9 and 12%, respectively. The result corroborated that Fe doping in the catalyst (forming a Ni–Fe alloy) could improve the catalyst stability, which promoted the SR reaction for the hydrogen production. For the common reforming, the concentrations of the products were relatively stable over the catalysts with different Fe loads, around 73% for H_2 and around 24% for CO_2. However, for the enhanced reforming, the CO_2 concentration showed an increasing trend with the increase in the Fe load, like the H_2 yield, to some extent corroborating that doping Fe in the catalyst could promote the oxidation of CO.

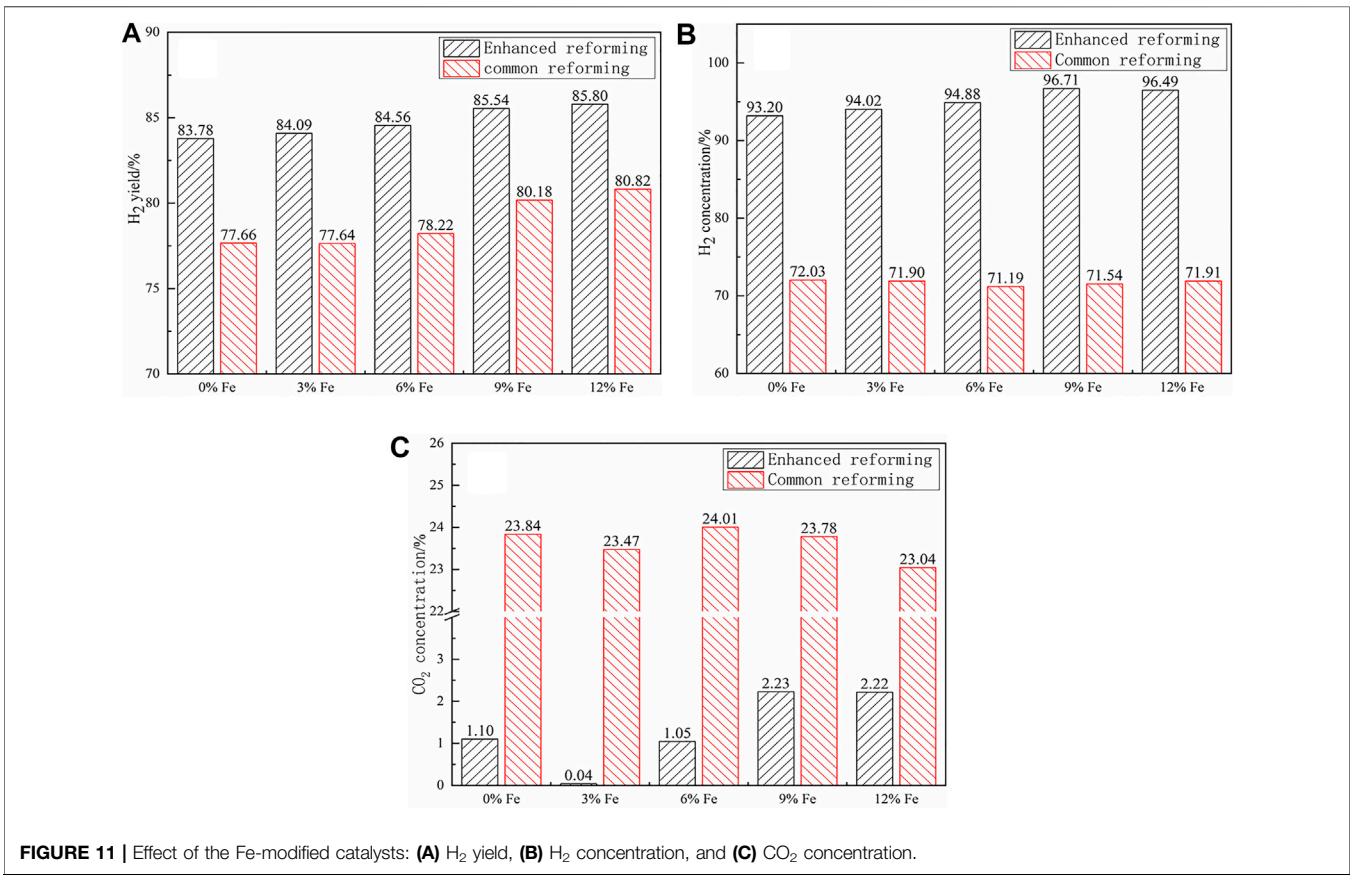

FIGURE 11 | Effect of the Fe-modified catalysts: **(A)** H_2 yield, **(B)** H_2 concentration, and **(C)** CO_2 concentration.

CONCLUSION

In this article, the double-effect Ni-based catalysts, modified with Ce, Mg, and Fe and synthesized by the coprecipitation method, were applied into the enhanced steam reforming process of real tar. The effects of the catalysts with different doping mass proportions (3, 6, 9, and 12%) of Ce, Mg, and Fe on the H_2 yield, and H_2 and CO_2 concentrations contrasted with those of the unmodified catalyst. The results revealed that the tar reforming efficiency was improved with appropriate proportion of the additives added. The Ce-doped catalyst, existing in the form of CeO_2, could change the distribution of the active component Ni and promote the thermal cracking and SR reactions. The modified catalyst with 6% Ce doping The Mg-doped catalyst, existing in the form of MgO and $MgNiO_2$, could change the morphology of Ni, increasing the catalytic area, which promoted the SR reaction. The best catalytic activity was obtained at 3% Mg doping, with the H_2 yield reaching 85.22%. The Fe-doped catalyst, existing in the form of Fe_2O_3, could form a Ni–Fe alloy and improve the stability of the catalyst, and the modified catalyst with 9 and 12% Fe doping showed the better catalytic activity, with the H_2 yield reaching 85.54 and 85.80%, respectively.

DATA AVAILABILITY STATEMENT

The original contributions presented in the study are included in the article/Supplementary Material; further inquiries can be directed to the corresponding authors.

AUTHOR CONTRIBUTIONS

PW and WZ conducted the experiments and wrote the manuscript. HX and ZY have corrected and edited the manuscript. MZ and ZW supported the project technically.

FUNDING

This research was financially supported by the Fundamental Research Funds for the Central Universities (N2025029), the National Natural Science Foundation of Liaoning Province (2019-MS-133), and the Open Project Program of Key Laboratory of Metallurgical Emission Reduction and Resources Recycling, Ministry of Education (Anhui University of Technology) (JKF19-06).

REFERENCES

Ashok, J., Kathiraser, Y., Ang, M. L., and Kawi, S. (2015). Bi-functional Hydrotalcite-Derived NiO-CaO-Al2O3 Catalysts for Steam Reforming of Biomass And/or Tar Model Compound at Low Steam-To-Carbon Conditions. *Appl. Catal. B: Environ.* 172-173, 116–128. doi:10.1016/j.apcatb.2015.02.017

Cai, W.-J., Qian, L.-P., Yue, B., and He, H.-Y. (2014). Rh Doping Effect on Coking Resistance of Ni/SBA-15 Catalysts in Dry Reforming of Methane. *Chin. Chem. Lett.* 25, 1411–1415. doi:10.1016/j.cclet.2014.06.016

Chan, F. L., and Tanksale, A. (2014). Review of Recent Developments in Ni-Based Catalysts for Biomass Gasification. *Renew. Sust. Energ. Rev.* 38, 428–438. doi:10.1016/j.rser.2014.06.011

Dou, B., Wang, C., Song, Y., Chen, H., Jiang, B., Yang, M., et al. (2016). Solid Sorbents for *In-Situ* CO 2 Removal during Sorption-Enhanced Steam Reforming Process: A Review. *Renew. Sust. Energ. Rev.* 53, 536–546. doi:10.1016/j.rser.2015.08.068

Duan, W., Yu, Q., Wang, K., Qin, Q., Hou, L., Yao, X., et al. (2015). ASPEN Plus Simulation of Coal Integrated Gasification Combined Blast Furnace Slag Waste Heat Recovery System. *Energ. Convers. Manage.* 100, 30–36. doi:10.1016/j.enconman.2015.04.066

Duan, W., Yu, Q., Wang, Z., Liu, J., and Qin, Q. (2018). Life Cycle and Economic Assessment of Multi-Stage Blast Furnace Slag Waste Heat Recovery System. *Energy* 142, 486–495. doi:10.1016/j.energy.2017.10.048

Duan, W., Yu, Q., Xie, H., and Qin, Q. (2017). Pyrolysis of Coal by Solid Heat Carrier-Experimental Study and Kinetic Modeling. *Energy* 135, 317–326. doi:10.1016/j.energy.2017.06.132

Furusawa, T., Saito, K., Kori, Y., Miura, Y., Sato, M., and Suzuki, N. (2013). Steam Reforming of Naphthalene/benzene with Various Types of Pt- and Ni-Based Catalysts for Hydrogen Production. *Fuel* 103, 111–121. doi:10.1016/j.fuel.2011.09.026

Gao, N., Liu, S., Han, Y., Xing, C., and Li, A. (2015). Steam Reforming of Biomass Tar for Hydrogen Production over NiO/ceramic Foam Catalyst. *Int. J. Hydrogen Energ.* 40, 7983–7990. doi:10.1016/j.ijhydene.2015.04.050

Gusta, E., Dalai, A. K., Uddin, M. A., and Sasaoka, E. (2009). Catalytic Decomposition of Biomass Tars with Dolomites. *Energy Fuels* 23, 2264–2272. doi:10.1021/ef8009958

Jiang, L., Hu, S., Wang, Y., Su, S., Sun, L., Xu, B., et al. (2015). Catalytic Effects of Inherent Alkali and Alkaline Earth Metallic Species on Steam Gasification of Biomass. *Int. J. Hydrogen Energ.* 40, 15460–15469. doi:10.1016/j.ijhydene.2015.08.111

Kimura, T., Miyazawa, T., Nishikawa, J., Kado, S., Okumura, K., Miyao, T., et al. (2006). Development of Ni Catalysts for Tar Removal by Steam Gasification of Biomass. *Appl. Catal. B: Environ.* 68, 160–170. doi:10.1016/j.apcatb.2006.08.007

Kinoshita, C. M., and Turn, S. Q. (2003). Production of Hydrogen from Bio-Oil Using CaO as a CO Sorbent. *Int. J. Hydrogen Energ.* 28 (10), 1065–1071. doi:10.1016/s0360-3199(02)00203-3

Koike, M., Li, D., Nakagawa, Y., and Tomishige, K. (2012). A Highly Active and Coke-Resistant Steam Reforming Catalyst Comprising Uniform Nickel-Iron alloy Nanoparticles. *ChemSusChem* 5, 2312–2314. doi:10.1002/cssc.201200507

Li, C., Hirabayashi, D., and Suzuki, K. (2009). A Crucial Role of O2– and O22– on Mayenite Structure for Biomass Tar Steam Reforming over Ni/Ca12Al14O33. *Appl. Catal. B: Environ.* 88, 351–360. doi:10.1016/j.apcatb.2008.11.004

Li, C., and Suzuki, K. (2010). Resources, Properties and Utilization of Tar. *Resour. Conservation RecyclingConservation Recycling* 54, 905–915. doi:10.1016/j.resconrec.2010.01.009

Li, D., Ishikawa, C., Koike, M., Wang, L., Nakagawa, Y., and Tomishige, K. (2013). Production of Renewable Hydrogen by Steam Reforming of Tar from Biomass Pyrolysis over Supported Co Catalysts. *Int. J. Hydrogen Energ.* 38, 3572–3581. doi:10.1016/j.ijhydene.2013.01.057

Li, D., Tamura, M., Nakagawa, Y., and Tomishige, K. (2015). Metal Catalysts for Steam Reforming of Tar Derived from the Gasification of Lignocellulosic Biomass. *Bioresour. Technol.* 178, 53–64. doi:10.1016/j.biortech.2014.10.010

Li, J., Tao, J., Yan, B., Jiao, L., Chen, G., and Hu, J. (2021). Review of Microwave-Based Treatments of Biomass Gasification Tar. *Renew. Sust. Energ. Rev.* 150, 111510. doi:10.1016/J.RSER.2021.111510

Mazumder, J., and de Lasa, H. I. (2015). Fluidizable La 2 O 3 Promoted Ni/γ-Al 2 O 3 Catalyst for Steam Gasification of Biomass: Effect of Catalyst Preparation Conditions. *Appl. Catal. B: Environ.* 168-169, 250–265. doi:10.1016/j.apcatb.2014.12.009

Mei, D., Lebarbier, V. M., Rousseau, R., Glezakou, V.-A., Albrecht, K. O., Kovarik, L., et al. (2013). Comparative Investigation of Benzene Steam Reforming over Spinel Supported Rh and Ir Catalysts. *ACS Catal.* 3, 1133–1143. doi:10.1021/cs4000427

Nakhaei Pour, A., and Mousavi, M. (2015). Combined Reforming of Methane by Carbon Dioxide and Water: Particle Size Effect of Ni-Mg Nanoparticles. *Int. J. Hydrogen Energ.* 40, 12985–12992. doi:10.1016/j.ijhydene.2015.08.011

Onozaki, M., Watanabe, K., Hashimoto, T., Saegusa, H., and Katayama, Y. (2006). Hydrogen Production by the Partial Oxidation and Steam Reforming of Tar from Hot Coke Oven Gas. *Fuel* 85, 143–149. doi:10.1016/j.fuel.2005.02.028

Richardson, Y., Blin, J., Volle, G., Motuzas, J., and Julbe, A. (2010). *In Situ* generation of Ni Metal Nanoparticles as Catalyst for H2-Rich Syngas Production from Biomass Gasification. *Appl. Catal. A: Gen.* 382, 220–230. doi:10.1016/j.apcata.2010.04.047

Sarıoğlan, A. (2012). Tar Removal on Dolomite and Steam Reforming Catalyst: Benzene, Toluene and Xylene Reforming. *Int. J. Hydrogen Energ.* 37, 8133–8142. doi:10.1016/j.ijhydene.2012.02.045

Tomishige, K., Kimura, T., Nishikawa, J., Miyazawa, T., and Kunimori, K. (2007). Promoting Effect of the Interaction between Ni and CeO2 on Steam Gasification of Biomass. *Catal. Commun.* 8, 1074–1079. doi:10.1016/j.catcom.2006.05.051

Torres, W., Pansare, S. S., and Goodwin, J. G. (2007). Hot Gas Removal of Tars, Ammonia, and Hydrogen Sulfide from Biomass Gasification Gas. *Catal. Rev.* 49, 407–456. doi:10.1080/01614940701375134

Virginie, M., Adánez, J., Courson, C., De Diego, L. F., García-Labiano, F., Niznansky, D., et al. (2012). Effect of Fe-Olivine on the Tar Content during Biomass Gasification in a Dual Fluidized Bed. *Appl. Catal. B: Environ.* 121-122, 214–222. doi:10.1016/j.apcatb.2012.04.005

Wang, L., Li, D., Koike, M., Koso, S., Nakagawa, Y., Xu, Y., et al. (2011). Catalytic Performance and Characterization of Ni-Fe Catalysts for the Steam Reforming of Tar from Biomass Pyrolysis to Synthesis Gas. *Appl. Catal. A: Gen.* 392, 248–255. doi:10.1016/j.apcata.2010.11.013

Wang, L., Li, D., Koike, M., Watanabe, H., Xu, Y., Nakagawa, Y., et al. (2013). Catalytic Performance and Characterization of Ni-Co Catalysts for the Steam Reforming of Biomass Tar to Synthesis Gas. *Fuel* 112, 654–661. doi:10.1016/j.fuel.2012.01.073

Wang, T., Chang, J., Cui, X., Zhang, Q., and Fu, Y. (2006). Reforming of Raw Fuel Gas from Biomass Gasification to Syngas over Highly Stable Nickel-Magnesium Solid Solution Catalysts. *Fuel Process. Technol.* 87, 421–428. doi:10.1016/j.fuproc.2005.10.006

Xie, H., Yu, Q., Yao, X., Duan, W., Zuo, Z., and Qin, Q. (2015). Hydrogen Production via Steam Reforming of Bio-Oil Model Compounds over Supported Nickel Catalysts. *J. Energ. Chem.* 24, 299–308. doi:10.1016/S2095-4956(15)60315-1

Xie, H., Yu, Q., Zhang, J., Liu, J., Zuo, Z., and Qin, Q. (2016a). Preparation and Performance of Ni-Based Catalysts Supported on Ca12 Al14 O33 for Steam Reforming of Tar in Coke Oven Gas. *Environ. Prog. Sust. Energ.* 36, 729–735. doi:10.1002/ep.12509

Xie, H., Yu, Q., Zuo, Z., Han, Z., Yao, X., and Qin, Q. (2016b). Hydrogen Production via Sorption-Enhanced Catalytic Steam Reforming of Bio-Oil. *Int. J. Hydrogen Energ.* 41, 2345–2353. doi:10.1016/j.ijhydene.2015.12.156

Xie, H., Yu, Q., Zuo, Z., Zhang, J., Han, Z., and Qin, Q. (2016c). Thermodynamic Analysis of Hydrogen Production from Raw Coke Oven Gas via Steam Reforming. *J. Therm. Anal. Calorim.* 126, 1621–1631. doi:10.1007/s10973-016-5638-9

Xie, H., Zhang, J., Yu, Q., Zuo, Z., Liu, J., and Qin, Q. (2016d). Study on Steam Reforming of Tar in Hot Coke Oven Gas for Hydrogen Production. *Energy Fuels* 30, 2336–2344. doi:10.1021/acs.energyfuels.5b02551

Xie, H., Zhang, W., Zhao, X., Chen, H., Yu, Q., and Qin, Q. (2018). Sorption-enhanced Reforming of Tar: Influence of the Preparation Method of CO2 Absorbent. *Korean J. Chem. Eng.* 35, 2191–2197. doi:10.1007/s11814-018-0136-3

Yue, B., Wang, X., Ai, X., Yang, J., Li, L., Lu, X., et al. (2010). Catalytic Reforming of Model Tar Compounds from Hot Coke Oven Gas with Low Steam/carbon Ratio over Ni/MgO-Al2O3 Catalysts. *Fuel Process. Technol.* 91, 1098–1104. doi:10.1016/j.fuproc.2010.03.020

Zamboni, I., Courson, C., and Kiennemann, A. (2011). Synthesis of Fe/CaO Active Sorbent for CO2 Absorption and Tars Removal in Biomass Gasification. *Catal. Today* 176, 197–201. doi:10.1016/j.cattod.2011.01.014

Zeng, X., Wang, F., Sun, Y., Zhang, J., Tang, S., and Xu, G. (2018). Characteristics of Tar Abatement by thermal Cracking and Char Catalytic Reforming in a Fluidized Bed Two-Stage Reactor. *Fuel* 231, 18–25. doi:10.1016/j.fuel.2018.05.043

Zhang, W., Xie, H., Wang, P., Li, R., Yu, Z., and Yu, Q. (2021a). Steam Reforming of Tar from Raw Coke Oven Gas over Bifunctional Catalysts: Effects of Preparation Parameters on CO 2 Adsorption Performance. *Environ. Prog. Sust. Energ.* 40, e13506. doi:10.1002/ep.13506

Zhang, W., Xie, H., Yu, Z., Wang, P., Wang, Z., and Yu, Q. (2021b). Steam Reforming of Tar from Raw Coke Oven Gas over Bifunctional Catalysts: Reforming Performance for H 2 Production. *Environ. Prog. Sust. Energ.* 40, e13501. doi:10.1002/ep.13501

Zuo, Z., Luo, S., Liu, S., Zhang, J., Yu, Q., and Bi, X. (2021). Thermokinetics of Mass-Loss Behavior on Direct Reduction of Copper Slag by Waste Plastic Char. *Chem. Eng. J.* 405, 126671. doi:10.1016/j.cej.2020.126671

Zuo, Z., Yu, Q., Luo, S., Zhang, J., and Zhou, E. (2020). Effects of CaO on Two-step Reduction Characteristics of Copper Slag Using Biochar as Reducer: Thermodynamic and Kinetics. *Energy Fuels* 34, 491–500. doi:10.1021/acs.energyfuels.9b03274

Conflict of Interest: The authors declare that the research was conducted in the absence of any commercial or financial relationships that could be construed as a potential conflict of interest.

Publisher's Note: All claims expressed in this article are solely those of the authors and do not necessarily represent those of their affiliated organizations, or those of the publisher, the editors and the reviewers. Any product that may be evaluated in this article, or claim that may be made by its manufacturer, is not guaranteed or endorsed by the publisher.